THE ORIGIN OF ENIGMATIC RIDGE NETWORKS, NILI FOSSAE, MARS: IMPLICATIONS FOR EXTENSIVE SUBSURFACE FLUID FLOW IN THE NOACHIAN. A. C. Pascuzzo[1], J. F. Mustard[1], E. Ebinger[1]
[1]Department of Earth, Environmental, and Planetary Science, Brown University, RI, 02912 USA (alyssa_pascuzzo@brown.edu)

Introduction: The origin of numerous, ~20-50 m wide, erosionally-resistant ridges (N_{total}≈16,000) observed and mapped in Noachian-aged terrain across a large region in Nili Fossae and the Nilosyrtis Highlands on Mars remains unresolved [1–9]. The ridges are on the order of 10 m high and 10's to 100's of km in length and exhibit diverse spatial relationships, including individual, isolated ridges, irregular polygonal ridge networks, and sub-parallel groupings [9]. Ridges are exposed by erosion or exhumation of the host rock in erosional windows, scarp walls, and crater floors. They are hosted in a Fe/Mg smectite-bearing, recessive, highly brecciated basement rock [2,4,5,10].

The morphology and geologic context the ridges suggests that surface processes (i.e., aeolian, fluvial, or glacial) are unlikely candidates for their formation [7–9]. Possible subsurface ridge formation mechanisms include: (1) volcanic diking along pre-existing fractures, (2) volcanic fill into pre-existing fractures [11], (3) breccia dikes from impact cratering [1,3], (4) clastic dikes, and (5) chemical alteration/precipitation of minerals in or along pre-existing fractures [2,4,7]. Each hypothesized formation mechanism implies different mineralogical suites possibly detectable in remotely sensed spectral data.

Previous studies used comparative morphology to assess formation hypotheses [1,7–9]. Here we summarize the results of new spectral and morphometric analyses [10] of the Nili Fossae ridge networks. HiRISE imagery and 8 CRISM scenes (**Fig.1a**) were used to map and isolate the spectral signatures of the ridges from their host unit and their physical characteristics (strike orientation and intersecting angles) to evaluate the hypothesized mechanisms responsible for ridge formation. We focus on the subset of ridges with good CRISM coverage and minimal dust. This subset (N_{subset}=819) dominantly displays irregular polygonal network patterns [9].

Morphometric Analysis: Ridge orientation and intersection angles were computed in ArcGIS for each ridge mapped in HiRISE and CTX imagery within and immediately around the CRISM scenes. Individual ridges were defined as continuous linear to curvilinear features with semi-consistent strike. Although curvilinear ridge's strike changes along their length we used a line between the start and end points of the ridge vector to approximate the mean orientation. Ridges that bend abruptly were mapped as two individual ridges.

Intersection angles between ridge segments were computed at the intersection point of two ridge vectors by subtracting the orientations of those branching segments.

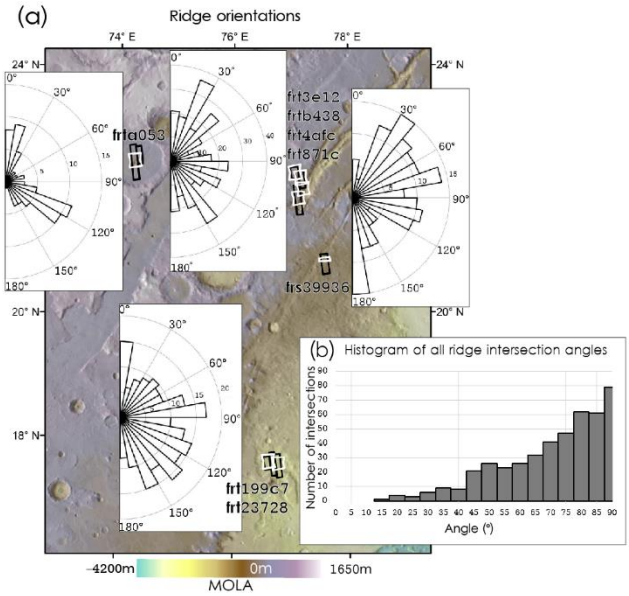

Fig.1 *(a) Rose diagrams of ridge orientations from HiRISE (black)/CTX imagery and associated group of CRISM scenes (white). (b) Histogram of all mapped ridge intersections.*

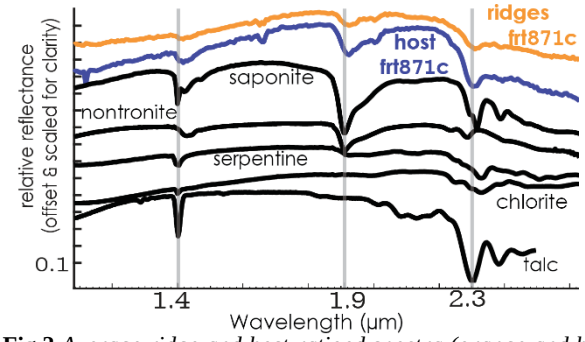

Fig.2 *Average ridge and host ratioed spectra (orange and blue, respectively). Plotted with lab spectra of Mg/Fe phyllosilicates.*

A branching segment is defined as a 30m sub-segment of each ridge vector from their intersection point.

Morphometric Results: Half-rose diagrams (**Fig.1a**) show the orientations of ridge networks in various locations across Nili Fossae. All locations show the ridges lack a dominant orientation except for one (FRTa053), which displays ridges with strong bimodal orientation (parallel and perpendicular to the Nili Fossae graben) and are being exhumed from sedimentary fill within the center of a crater (22.45°N, 74.30°E). The networks display a range of intersection angles with a strong tendency towards near-orthogonal T-junctions (**Fig.1b**). The percentage of mutually intersecting ridges is >80% in the study area. The average intersecting angle is ~68º with a standard deviation of ~17º and a mode of 89º.

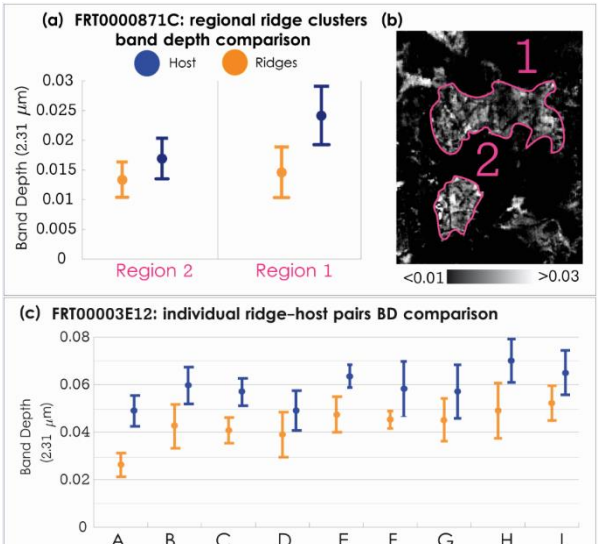

Fig.3 *(a) Mean 2.31 μm BDs for ridges and host rock for ridge clusters with standard deviation (bars) from 2 outcropped regions in (b) FRT871c's BD map. (c) Mean BDs plotted for 9 (A-I) individual ridges and adjacent host material in FRT3e12.*

Spectral Analysis: [10]'s detailed analysis of the near-infrared spectra of the ridges and their host unit found the ridges share all of the diagnostic spectral features of Mg-smectite and/or mixed-layered talc-smectite clays of the host materials (**Fig.2**). Spectral analysis methods are summarized in [10]. The key spectroscopic differences are (1) ridges display consistently weaker absorptions near 1.4, 1.9, and 2.31 μm and (2) the spectral slope at longer wavelengths is shallower compared to the host spectra (**Fig.2**).

Our new spectral analyses used averages of the calculated band depth (BD) at 2.31 μm [12] extracted from well-exposed ridge clusters (**Fig.3a; 3b**) and individual ridges (**Fig.3c**) compared to their immediate host rock's for two CRISM scenes, FRT871C and FRT3E12. On average, the ridges' 2.31 μm band strength is weaker than the host by 0.5-3% and 1-2.5% for the ridge clusters and individual ridges, respectively. Student t tests between the BDs of clusters or individual ridges and the average host BDs shows the difference is statistically significant within 99% confidence, regardless of spatial scale.

Formation Mechanisms: Ridge orientation and intersecting angles can be used to interpret the state of stress during their formation. Their irregular polygonal nature, near-orthogonal intersections, and lack of a dominant orientation are characteristics consistent with fracture propagation under horizontal near-isotropic extensional stress in a physically heterogeneous host rock [13,14]. Variance in ridge orientation and distribution implies that the fractures propagated with respect to local stresses more so than regional stresses with multiple generations of fractures under varying stress fields.

The results from the spectral analysis suggest the ridges are composed of similar clay-bearing material to the host. The weaker band strength associated with the ridges could be due to large grain size as expected with lithified sediment. This could explain compositional similarity but different physical properties. Additionally, ridges could be cemented or lithified with a mineral that is spectrally inactive across VNIR wavelengths (e.g., quartz, silica polymorphs, some oxide group minerals, and amorphous materials), that would dampen the spectral features caused by VNIR active minerals.

The ridges' geometry and spectral properties suggest cementation/lithification along fracture zones and fracture fill or shallow clastic diking into the pre-existing subsurface fractures as the favored hypothesis in a uniform stress field. This would lead to resistant irregularly polygonal ridges spectrally similar to the Noachian basement.

Igneous processes and impact-induced fracturing and breccia injection are unlikely formation processes. The ridge geometries are inconsistent with those of terrestrial magmatic dikes, which commonly form in parallel swarms or radially (in a horizontal isotropic regime) [15,16]. Additionally, igneous dike swarms are not observed forming dense polygonal networks even in regions where shallow intrusion into a physically heterogeneous crust or multiple intrusion events have occurred [17]. And unless these ridges were formed during the Isidis event, they are not likely to be impact-generated fractures and breccia dikes.

Our results support the presence of extensive subsurface groundwater activity following the Isidis event. Evidence for this groundwater activity is preserved in the ridges observed throughout the region. The ridge hosting basement unit warrants further investigation to understand the specific origin and development of the pre-existing fractures and source of the ridge material. Improved spectral analyses would require DISORT-based atmospheric and aerosol correction [18], nonlinear spectral unmixing based on Hapke radiative transfer modeling, and/or modified sparse unmixing methods [19]. Such analyses would help narrow down the mineralogic differences between the Noachian basement and the ridges in Nili Fossae.

References: [1] Head, J. W. & Mustard, J. F. (2006) *MPS*, *41*, 1675–1690; [2] Mangold, N. et al. (2007) *JGR.*, *112;* [3] Mustard, J. F. et al. (2007) *JGR.*, *112;* [4] Mustard, J. F. et al. (2009) *JGR.*, *114;* [5] Ehlmann, B. L. et al. (2009) *JGR*, *114;* [6] Ivanov, M. A., et al. (2012) *Icarus*, *218*, 24–46; [7] Saper, L. & Mustard, J. F. (2013) *GRL*, *40*, 245–249; [8] Ebinger, E. K. & Mustard, J. F. (2015), *46th LPSC*, #2034; [9] Ebinger, E. K., & Mustard, J. F. (2016), *47th LPSC*, #2731; [10] Pascuzzo, A. C., & Mustard, J. F. (2017), *48th LPSC*, #2807; [11] Kerber, L. et al. (2017) *Icarus*, *281*, 200–219; [12] Pelkey, S. M. et al. (2007) *JGR*, *112*, E08S14; [13] Lonergan, L. et al. (1998) *JSG*, *20*, 529–548; [14] Tuckwell, G. W. et al. (2003) *JSG*, *25*, 1241–1250; [15] Delaney, P. T. & Pollard, D. D. (1981) U.S. G.P.O.; [16] Smith, R. P. et al. (1987) *Geol. Assoc. Can. Spec. Pap.*, *34*, 47–54; [17] Le Gall, B. et al. (2005) *JSG.*, *27*, 2234–2255; [18] McGuire, P. C., et al. (2008) *IEEE Trans. Geosci. Remote Sens.*, *46*, 4020–4040; [19] Lin, H. & Zhang, X. (2017) *Icarus*, *288*, 160–171.